Received: 16 September 2020 | Revised: 7 December 2020 | Accepted: 12 December 2020

DOI: 10.1002/hipo.23296

WILEY

RESEARCH ARTICLE

Adult-born granule cell mossy fibers preferentially target parvalbumin-positive interneurons surrounded by perineuronal nets

Brandy A. Briones[1,2] | Thomas J. Pisano[1] | Miah N. Pitcher[1] | Amanda E. Haye[1,2] | Emma J. Diethorn[1,2] | Esteban A. Engel[1] | Heather A. Cameron[3] | Elizabeth Gould[1,2]

[1]Princeton Neuroscience Institute, Princeton University, Princeton, New Jersey

[2]Department of Psychology, Princeton University, Princeton, New Jersey

[3]Section on Neuroplasticity, National Institute of Mental Health, National Institutes of Health, Bethesda, Maryland

Correspondence
Elizabeth Gould, Princeton Neuroscience Institute, Princeton University, Princeton, NJ 08544.
Email: goulde@princeton.edu

Funding information
Division of Graduate Education, Grant/Award Number: DGE-1656466; National Institute of Mental Health, Grant/Award Numbers: MH117459-01, MH118631-01, ZIAMH002784; National Institute of Neurological Disorders and Stroke, Grant/Award Number: F31 NS089303; Princeton Neuroscience Institute, Innovation Fund

Abstract

Adult-born granule cells (abGCs) integrate into the hippocampus and form connections with dentate gyrus parvalbumin-positive (PV+) interneurons, a circuit important for modulating plasticity. Many of these interneurons are surrounded by perineuronal nets (PNNs), extracellular matrix structures known to participate in plasticity. We compared abGC projections to PV+ interneurons with negative-to-low intensity PNNs to those with high intensity PNNs using retroviral and 3R-Tau labeling in adult mice, and found that abGC mossy fibers and boutons are more frequently located near PV+ interneurons with high intensity PNNs. These results suggest that axons of new neurons preferentially stabilize near target cells with intense PNNs. Next, we asked whether the number of abGCs influences PNN formation around PV+ interneurons, and found that near complete ablation of abGCs produced a decrease in the intensity and number of PV+ neurons with PNNs, suggesting that new neuron innervation may enhance PNN formation. Experience-driven changes in adult neurogenesis did not produce consistent effects, perhaps due to widespread effects on plasticity. Our study identifies abGC projections to PV+ interneurons with PNNs, with more presumed abGC mossy fiber boutons found near the cell body of PV+ interneurons with strong PNNs.

KEYWORDS
adult neurogenesis, hippocampus, mossy fibers, perineuronal nets, plasticity

1 | INTRODUCTION

A large body of evidence has demonstrated that adult neurogenesis contributes to the function of the mammalian hippocampus. Adult-born granule cells (abGCs) integrate into the preexisting circuitry, participating in hippocampus-dependent functions such as learning, adaptability, and feedback of the stress response (Abrous & Wojtowicz, 2015; Akers et al., 2014; Laplagne et al., 2006; Sahay et al., 2011; Snyder, Soumier, Brewer, Pickel, & Cameron, 2011). This process is susceptible to environmental influences, suggesting that abGC microcircuitry may serve as a substrate for experience-dependent change in hippocampal function (Llorens-Martín, Jurado-Arjona, Avila, & Hernández, 2015; Opendak et al., 2016; Sah, Peterson, Lubejko, Vivar, & van Praag, 2017; Schoenfeld, Rada, Pieruzzini, Hsueh, & Gould, 2013; van Praag, Kempermann, & Gage, 1999; Vivar, Peterson, & van Praag, 2016). Shortly after their generation, abGCs form dendrites and mossy fiber axons, communicating with neighboring mature granule cells (Dieni, Gonzalez, & Overstreet-Wadiche, 2019; Luna et al., 2019) in addition to extending into the hilus where they ramify and target several cell types including

pyramidal cells of the CA2/CA3 regions, hilar mossy cells, and interneurons of the CA2/CA3 regions and dentate gyrus (DG) (Llorens-Martín et al., 2015; Toni et al., 2008).

Evidence suggests that parvalbumin-expressing (PV+) interneurons, the most abundant interneuron subtype in the hippocampus (Freund & Buzsáki, 1996), receive inputs from abGCs (Marín-Burgin, Mongiat, Pardi, & Schinder, 2012; Song et al., 2013). PV+ cells reciprocally synapse onto abGCs, creating a feedforward inhibitory circuit important for modulating DG excitability and pattern separation (Ikrar et al., 2013; Sahay et al., 2011). These studies, however, have treated PV+ interneurons as a relatively homogeneous group, despite the fact that a significant proportion, but not all, of PV+ cells are surrounded by perineuronal nets (PNNs) (Dityatev et al., 2007; Lensjø, Christensen, Tennøe, Fyhn, & Hafting, 2017; Schüppel et al., 2002), specialized extracellular matrix structures known to modulate physiological and structural plasticity (Favuzzi et al., 2017; Sorg et al., 2016). In the developing visual cortex, PNNs surrounding PV+ interneurons reduce plasticity, which leads to closure of the critical period for ocular dominance (Hou et al., 2017; Pizzorusso et al., 2002). PNNs also facilitate synaptic and behavioral plasticity by enhancing feedback inhibition of hippocampal PV+ interneurons (Shi et al., 2019). Together, these studies suggest that PNNs surrounding PV+ interneurons play complex roles, which may differ depending on region and developmental stage.

In the DG, PNNs surround the majority of PV+ cells (Lensjø et al., 2017), and, of these, the majority are likely basket cells (Jansen, Gottschling, Faissner, & Manahan-Vaughan, 2017), as PV+ bistratified interneurons also express somatostatin which does not colocalize with PNNs (Murthy et al., 2019). While it is well-established that DG PV+ interneurons receive inputs from abGCs, the potential influence of PNNs has not been previously explored. To investigate this relationship, we examined the mossy fibers of abGCs using GFP-retroviral labeling and endogenous immature neuron marker microtubule protein 3-Repeat-Tau (3R-Tau), and their proximity to DG PV+ interneurons surrounded by varying intensities of PNNs.

We found that abGC mossy fibers were more abundant near DG PV+ interneurons with intense PNNs than those with no or weak PNNs. Among the PV+ PNN+ population, we found that cells with more intense PNN labeling were more likely to have abGC mossy fiber boutons nearby than those with weaker labeled PNNs. This result raises the possibility that abGC connectivity influences PNN formation, in addition to the possibility that PNN components attract and stabilize abGC mossy fibers. To investigate whether the presence of abGCs influences PNN formation, we analyzed PNNs in three different conditions associated with altered levels of adult neurogenesis: (a) transgenic inhibition of adult neurogenesis, (b) age-related decline of adult neurogenesis, and (c) exercise-induced enhancement of adult neurogenesis. Transgenic depletion of abGCs was associated with reduced PV+ interneurons that were PNN+ and reduced PNN intensity, but consistent relationships between the number of abGCs and PV+ PNN+ interneurons were not observed in the experiential conditions. Together these results indicate that new neurons preferentially innervate PV+ interneurons surrounded by intense PNNs, but that new neuron innervation may alter PNN formation only under conditions of specific, near complete, elimination of abGCs.

2 | MATERIALS AND METHODS

2.1 | Animals and experimental design

All animal procedures were conducted in accordance with the National Institutes of Health guidelines and approved by the Princeton University Institutional Animal Care and Use Committees. All mice were housed five to a cage, with the exception of the running experiment, under a reverse 12-hr light–dark schedule (lights off at 0700) with free access to food and water. Male C57BL/6J mice aged 5–7 weeks upon arrival from The Jackson Laboratory (Bar Harbor, ME) (strain #000664) were used for retroviral labeling. Male C57BL/6J mice from The Jackson Laboratory were also used for 3R-Tau labeling (aged 7–11 weeks at the time of perfusion) and the age-related decline study (perfused at 5 weeks for young adult mice and 16 weeks for middle-aged adult mice). Transgenic mice, expressing HSV-TK under the GFAP promoter, and their wildtype CD1 littermates (NIMH, Bethesda, MD), were treated for 10.5 weeks with valganciclovir (vgcv, p.o., 227 mg/kg chow, 4 days/week) and perfused at age 19–20 weeks. Mice in the running study were male C57BL/6J bred in-house; housed two mice per cage to avoid overcrowding and fighting that occurs when a running wheel is shared by multiple mice (Howerton, Garner, & Mench, 2008; Kaliste, Mering, & Huuskonen, 2006). Runners were housed for 4 weeks with ad libitum access to a wireless running wheel (Med Associates Inc., Fairfax, VT) beginning at 6 weeks of age, and controls were housed for 4 weeks with a locked wireless running wheel. At the conclusion of each experiment, mice were deeply anesthetized with 0.07 ml Euthasol (i.p. injection) and transcardially perfused with 4.0% paraformaldehyde (PFA) in phosphate buffered saline (PBS), pH 7.5. The brains were dissected and postfixed in 4.0% PFA for 48 hr before processing.

2.2 | Production of viral vector

A replication-deficient retroviral vector based on the Moloney leukemia virus and expressing GFP from the CAG promoter, was used to specifically transduce abGCs, as described previously (Zhao, Teng, Summers, Ming, & Gage, 2006). Retroviral particles were produced and purified at the Princeton Viral Core at the Princeton Neuroscience Institute, as previously described (Sullivan & Wickersham, 2015). Briefly, a mix of three plasmids were co-transfected over HEK293T cells and viral particles were purified by a sucrose step gradient. Plasmid CAG-GFP (Addgene #16664), was a gift from Fred Gage (Zhao et al., 2006). Plasmid pCI-VSVG (Addgene #1733), was a gift from Garry Nolan. Plasmid pUMVC (Addgene #8449), was a gift from Bob Weinberg (Stewart et al., 2003). Virus titer of 4×10^5 transducing units/ml was determined after transduction of polybrene-treated murine fibroblasts and quantification of GFP-expressing cells.

2.3 | Stereotaxic surgery for retroviral delivery

Mice were between 5 and 7 weeks of age at the time of surgery, and were anesthetized with 1–2% isoflurane and placed in a stereotaxic setup (Kopf, Tujunga, CA). A microsyringe was used to deliver retrovirus bilaterally to the dorsal DG (1.0 μl per injection at 0.15 μl/min) using stereotaxic coordinates according to Paxinos and Franklin's (2008) mouse brain atlas from bregma (mm): −2.0 anteroposterior, ±1.3 lateral, −2.0 dorsoventral (suprapyramidal blade); −2.0 anteroposterior, ±1.3 lateral, −2.3 dorsoventral (infrapyramidal blade). Mice were perfused 3 or 6 weeks post-infection (wpi) for histochemical labeling and confocal imaging (Figure S1a,b).

2.4 | Histology

All histochemistry was carried out on 50 μm-thick free floating coronal brain sections, for example sections see Figure S1b. Sections were incubated in various combinations of primary antibodies against GFP, 3R-Tau, Synaptophysin, PSA-NCAM, and PV, and biotinylated lectin *Wisteria floribunda agglutinin* (WFA), a plant-based lectin commonly used to label PNNs, at 4°C for 48 hr in 0.1 M PBS with 0.3% Triton X-100 and 3% normal donkey serum. After incubation in primary antisera, sections were washed and placed in secondary antisera in 0.1 M PBS with 0.3% Triton X-100 for 2 hr at room temperature. All labeled brain sections were counterstained with DAPI. For a detailed list of antibodies used, see Table 1. For the PSA-NCAM, PV, and PNN density analyses in the GFAP-TK experiment, whole sections were imaged with a Hamamatsu NanoZoomer S60 (Japan). Sections from all other experiments were imaged with a Zeiss confocal microscope LSM 700 (Oberkochen, Germany).

2.5 | Confocal microscopy

Images were acquired using a Zeiss confocal microscope (LSM 700; four visible solid-state lasers: UV 405; argon 458/488; HeNe 555/568; far-red 639). For intensity and bouton analysis of abGC mossy fibers, triple-labeled sections for abGC mossy fibers, GFP or 3R-Tau (depending on the experiment), PV, and WFA were imaged. Only brain sections with visible GFP or 3R-Tau mossy fiber staining were scanned. From these sections, all PV+ cells in the hilus and sgz of the DG were scanned. Images of labeled cells focused on single PV + cell bodies and proximal dendrites and were acquired (×63 with ×2 zoom; NA, 1.4; oil-immersion) by taking z-stacks, including the entirety of the cell body ±10 μm above and below the cell body surface using 0.05 μm z-plane intervals (>300 optical slices per cell).

For intensity analysis of PNNs in the GFAP-TK experiment, PV and WFA labeling were imaged same as described for the GFP and 3R-Tau experiments. For an unbiased analysis of PNN intensity, imaging of PV+ cells were randomly sampled from those in the PV channel, only (n = 42 cells; 6 cells per brain), by an experimenter blinded to condition. Brain sections for comparison were stained together and taken with identical confocal settings to allow for cross comparison of optical intensities.

For the GFP and 3R-Tau paired analysis, approximate PV+ cell location was recorded separately on a dorsal hippocampus template to locate neighboring pairs (defined as ≤ 30 μm distance apart). Neighboring PV+ cells, where one cell was comparatively greater in PNN expression than its neighbor, were first selected visually by the investigators. Visual selection of neighboring PV+ cells provided an unambiguous distinction between higher and lower PNN expressing cells. The selected opposing pairs were then validated by comparing their respective PNN optical intensities; only those pairs where one cell was below the lower 95% confidence interval of the mean for PNN

TABLE 1 Reagent resource table

Name	Host species	Dilution	Type	Company	Catalog #	RRID #
Parvalbumin (PV)	Mouse	1:500	Primary	Sigma-Aldrich (St. Louis, MO)	P3088	AB_477329
Parvalbumin (PV)	Rabbit	1:2000	Primary	Abcam (Cambridge, UK)	ab11427	AB_298032
GFP	Rabbit	1:500	Primary	Molecular Probes (Eugene, OR)	G10362	AB_2536526
Wisteria floribunda agglutinin (WFA) lectin	N/A	1:500	Primary	Sigma-Aldrich	L1516	AB_2620171
3RTau	Mouse	1:500	Primary	Millipore (Burlington, MA)	05-803	AB_310013
Synaptophysin (SYP)	Mouse	1:200	Primary	Millipore	MAB329	AB_94786
PSA-NCAM	Rat	1:400	Primary	BD Pharmingen (San Diego, CA)	556325	AB_396363
Donkey anti-mouse 568	Donkey	1:500	Secondary	Invitrogen (Carlsbad, CA)	A10037	AB_2534013
Donkey anti-rat 488	Donkey	1:500	Secondary	Abcam	ab150153	AB_2737355
Donkey anti-rabbit 488	Donkey	1:500	Secondary	Invitrogen	A21206	AB_2535792
Donkey anti-rabbit 568	Donkey	1:500	Secondary	Invitrogen	A10042	AB_2534017
Anti-streptavidin 647	N/A	1:500	Secondary	Molecular Probes	S21374	AB_2336066
Anti-streptavidin 488	N/A	1:500	Secondary	Molecular Probes	S11223A	AB_2315383

intensity (3 wpi: 395.45, 6 wpi: 606.77, 3R-Tau: 893.63) and the other cell was above the upper 95% confidence interval of the mean (3 wpi: 580.14, 6 wpi: 967.11, 3R-Tau: 1,089.71) were included in the analysis. See examples of neighboring PV+ PNN negative-to-low (neg-low) and PV+ PNN high intensity cells in Figure 1c.

For PSA-NCAM+, PV+ PNN+, and PNN+ cell density analyses, images of the entire dorsal DG were acquired (×20 with ×0.5 zoom; NA, 0.8) taking z-stacks at 3.0 μm intervals (~15 optical slices). All slides were coded prior to analysis and the code was not revealed until the analysis was complete.

2.6 | Analysis of confocal images

In order to detect abGC mossy fiber labeling at various distances from the PV+ cell edge, we designed an analysis pipeline to preprocess the

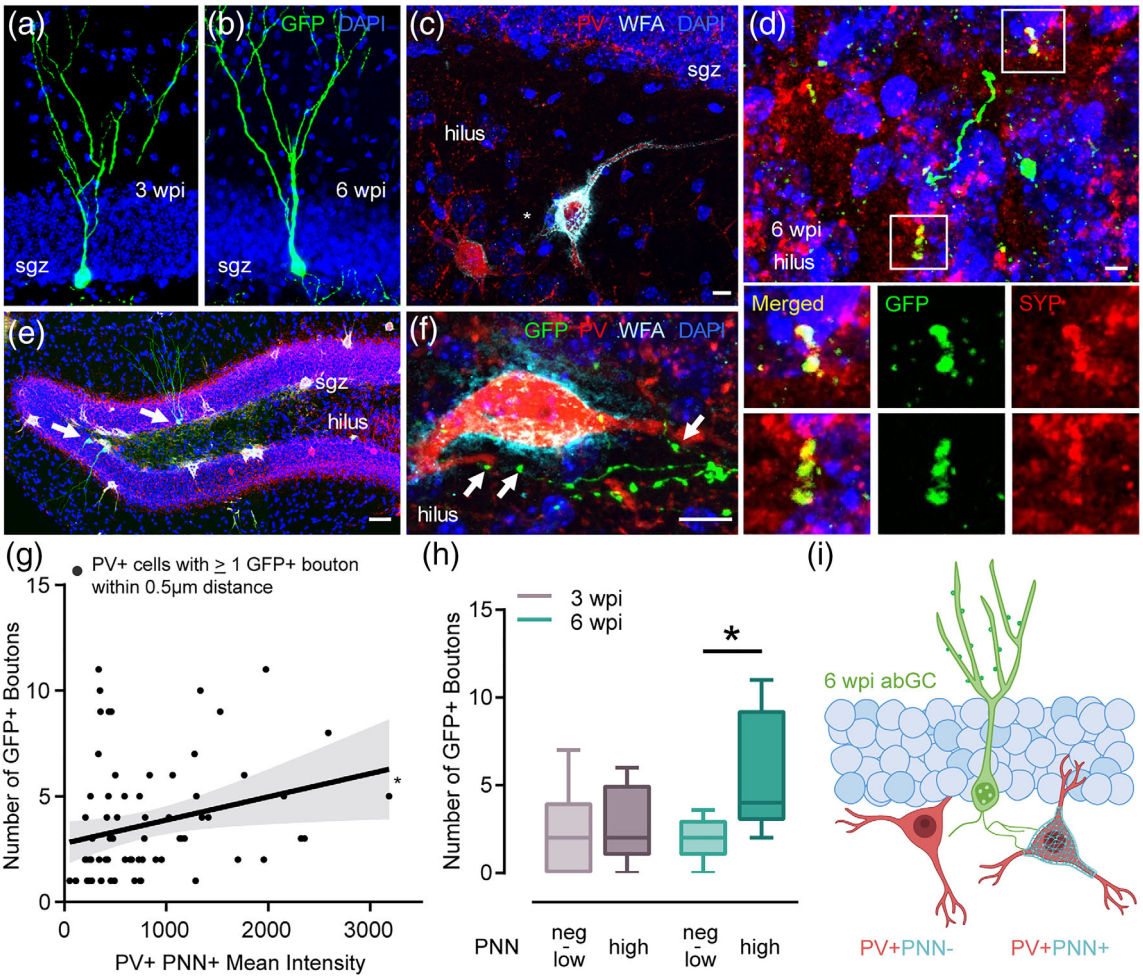

FIGURE 1 abGC mossy fiber boutons at 6 wpi are more abundant near PV+ interneurons surrounded by intense PNNs compared to neighboring PV+ interneurons with weak PNNs. (a–b) Adult mice (n = 10) were injected with retrovirus CAG-GFP (green) in the DG. Representative high magnification images of a 3 wpi abGC (a) and 6 wpi abGC (b). (c) Representative high magnification image of neighboring PV+ interneurons (red) in the hilus, where one is enwrapped in WFA+ PNN (white-cyan; indicated with a white asterisk) and the other is not. Scale bar = 10 μm. (d) Representative high magnification image of adult-generated mossy fibers and boutons (GFP; green), presynaptic protein, synaptophysin (SYP; red), and counterstain (DAPI; blue) in the hilus at 6 wpi. Examples of colabeled boutons are boxed. Merged images show colabeled GFP and SYP boutons. Scale bar = 5 μm. (e) Representative image of adult-born neurons infected with GFP-retrovirus (green; indicated by white arrows), PV+ interneurons (red), WFA+ PNNs (white-cyan), and DAPI (blue). Scale bar = 50 μm. (f) Representative high magnification image of GFP+ abGC mossy fibers (green) proximal to a PV+ PNN+ interneuron. Examples of GFP+ abGC boutons indicated by white arrows. Scale bar = 10 μm. (g) Positive correlation between PV+ interneuron WFA+ PNN optical intensity and number of GFP+ abGC boutons from both 3 and 6 wpi abGCs, combined (r = .2632, p = .0255). (h) Paired t test comparison of GFP+ abGC mossy fiber bouton number within 0.5 μm of the PV+ cell surface, between pairs of PV+ interneurons located close together where one cell has either negative-to-low intensity PNNs (neg-low) and the other has high intensity PNNs (high). No differences were found at 3 wpi (t_{26} = 0.4642, p = .6465). At 6 wpi, greater numbers of boutons surrounded high intensity PNN+ PV+ interneurons compared to neighboring neg-low intensity PNN+ PV+ interneurons (t_{15} = 3.784, p = .0018). Data are presented as 10–90 percentile box and whisker plots. (i) Conceptual schematic of a 6 wpi abGC sending more axon projections to a PV + PNN+ interneuron compared to the neighboring PV + PNN− interneuron. *p < .05. Related to Figure S1 [Color figure can be viewed at wileyonlinelibrary.com]

z-stack confocal images (details below), segment fluorophore signal from markers for GFP, 3R-Tau, PV, or WFA, and analyze the optical intensity of the signal (Figure S1c). Analyses of mossy fibers and PNNs surrounding PV+ cells were conducted using custom Python software (available upon request). Image loading was performed using Scikit-Image 0.13.11 (van der Walt et al., 2014) and SimpleITK 1.0.0 (Lowekamp, Chen, Ibáñez, & Blezek, 2013). Statistical analyses were performed using SciPy 1.1.0 (Virtanen et al., 2020). Data manipulations were performed in Python 2.7 using Numpy 1.14.3 (Harris et al., 2020) and Pandas 0.23.0 (McKinney, 2010). Blinding to condition was maintained during this process.

2.7 | Analysis pipeline

To control for heterogeneity in staining across the different labels used (GFP, 3R-Tau, PV, WFA), we first developed parameters for each in order to produce an overall analysis preprocessing pipeline. Thresholds for each label were determined empirically from optical intensity distributions. The preprocessing pipeline was developed using machine learning image segmentation which developed label-specific parameters for optimal signal detection. Segmentation within each channel, as described below, was carried out for accurate signal detection, and was validated by two human experimenters by comparing overlays of the raw image with the segmented image. In cases where the segmentation process did not produce results that were at least 90% accurate, the parameters were improved and the segmentation process was carried out again until the preprocessing produced results that matched those of the human experimenters for the vast majority of cells (retrovirus experiment: 96.7%; 3R-Tau experiment: 94.7%). For a small percentage of images (retrovirus experiment: 3.3%; 3R-Tau experiment: 5.3%), the raw image did not correspond to the segmented image. These cells were removed from all analyses. It should be noted that the few cases where the segmentation process did not match detection by human experimenters were due to problems with the raw data, for example, nonspecific staining or oversaturation in the raw image, and not for an inexplicable reason potentially related to flaws in the analysis preprocessing pipeline. After completing this process, a series of preprocessing parameters were finalized, including the number of iterations, Gaussian filters, voxel kernels, and thresholds, each particular to the label/fluorophore/channel to be analyzed.

PV+ cell segmentation: PV+ signal volumes were preprocessed through a series of Gaussian filtering (21 voxel kernel), eroding, and dilating (nine voxel kernel each). Voxels with intensities below 0.8 *SD* from the mean were set to zero. *Mossy fiber segmentation*: GFP+ or 3R-Tau+ signal, depending on the experiment, went through one iteration of Gaussian filtering (3 voxel kernel), eroding and dilating (3 voxel kernel each). Threshold was set at 1.0 *SD* above the mean. *PNN segmentation*: WFA+ signal went through two iterations of Gaussian filtering (25 voxel kernel), eroding, and dilating (nine voxel kernel each). Threshold was set at 0.8 *SD* above the mean. *Cell edge detection and ring analysis*: After preprocessing, voxel-wise distances from the detected PV+ cell edge were calculated (scipy.ndimage.morphology.distance_transform_edt). The region of interest for abGC mossy fiber intensity analysis was set to a maximum distance of 0.25 μm from the PV+ cell edge. Corresponding PV+ intensity and WFA+ PNN intensity values were plotted and Pearson's correlation coefficient (r) was computed to assess the relationship between mossy fiber labeling, PNN intensity, and the relevant PV+ cell.

2.8 | Mossy fiber bouton analysis

To obtain a more specific measure of putative mossy fiber terminals, we carried out analyses on z-stack confocal images of single PV+ cell bodies and proximal dendrites, acquired (×63 with ×2 zoom; NA, 1.4; oil-immersion) by taking z-stacks including the entirety of the PV+ cell body ±10 μm above and below the cell body surface, using 0.05 μm z-plane intervals (>300 optical slices per cell), using shape and volumetric criterion for mossy fiber boutons: spherical/puncta shape with a $3.0\mu m^3 \leq \times \leq 50.0\ \mu m^3$ volume (Toni et al., 2008). We used a connected components analysis (scipy.ndimage.measurements.label) revealing grouped islands of nonzero voxels. Centers of mass (scipy.ndimage.measurements.center_of_mass) were then recorded for cell center and mossy fiber puncta. Individual voxel-wise Euclidean distances between edges of mossy fiber puncta and the PV+ cell edge were calculated, where the voxel pair with the shortest distances were recorded. Post-processed mossy fiber puncta voxel intensity means and sums were also recorded. Only mossy fiber puncta values with the specified shape and volume criterion, described above, and a Euclidean distance ≤ 0.5 μm from the PV+ cell edge were recorded. Mossy fiber bouton number and corresponding PV+ and WFA+ PNN intensity values were plotted. Pearson's correlation coefficient (r) was computed to assess the relationship between mossy fiber boutons and the relevant PV+ cell.

2.9 | Cell density, intensity, and statistical analysis

Cell densities for PSA-NCAM+, PV+, and/or PNN+ cells were counted using FIJI (FIJI is just ImageJ, NIH; Schindelin et al., 2012), except for the GFAP-TK experiment, which was counted using the NanoZoomer Digital Pathology viewing software (NDP view2 Plus, Hamamatsu). Both were calculated by dividing the total number of positive-labeled cells within the dorsal hilus and sgz of the DG over the traced volume. Volumes were traced from max projections in the DAPI channel by researchers unaware of the experimental groups. Percent colocalization of PV+ cells surrounded by PNNs was determined by calculating total number of PV+ PNN+ cells over the total number of PV+ cells. Density and colocalization comparisons between groups were statistically analyzed using either linear mixed effects (lme) modeling using the lme4 package (Bates et al., 2015) in RStudio (RStudio Team, 2020), or unpaired *t* tests (with or without corrections for unequal *SD*). Datasets with multiple dependent variable values per animal were taken into account in lme models to prevent over-averaging errors. Statistics used include lme modeling, Pearson

r correlations, simple linear regressions, and one sample, paired, and unpaired *t* tests, as described throughout the text, Figure and Supplementary Figure Legends, and Statistics Tables. Unless otherwise stated, midlines on box and whisker plots are presented as the median. Outliers were assessed using a robust regression and outlier removal (ROUT) method (Q = 0.2%) in GraphPad Prism 9.0.0 (GraphPad Software, San Diego, CA) for single-value dependent variables, see Supplementary Tables. Outliers were assessed using the box plot statistics function, boxplot.stats, in RStudio for multiple-value dependent variables, where five outliers were excluded in the aging study, see Table S4. Non-normal datasets were analyzed using nonparametric tests. Normality was assessed using Anderson-Darling test, Shapiro–Wilk test, D'Agostino & Pearson omnibus test, and Kolmogorov–Smirnov test, with a p value of .05. All code and data that support the findings of this study are available from the corresponding author upon request.

3 | RESULTS

3.1 | Adult-generated mossy fiber boutons are more numerous near PV+ neurons surrounded by PNNs

GFP-retrovirus injection in the DG of adult mice at both 3 and 6 weeks post-infection (wpi) produced consistent labeling of cells with granule cell morphology in both the suprapyramidal and infrapyramidal blades of the granule cell layer (Figure 1a,b,e). GFP-labeled mossy fibers were observed emanating from GFP-labeled granule cells into the hilar region, and had characteristic varicosities known to represent *en passant* synapses (Toni et al., 2008; Zhao et al., 2006). These GFP-labeled varicosities were often observed in close proximity to PV+ cells in the DG (Figure 1f). We verified whether these GFP+ boutons were likely sites of synaptic contact with the presynaptic marker synaptophysin, and found positive evidence of colabeling (Figure 1d). In order to detect abGC mossy fiber bouton labeling near PV+ interneurons, we created a 0.5 μm ring surrounding the PV+ cell edge as our region of interest (ROI) for analysis. Using our analysis pipeline to preprocess z-stack confocal images, we segmented fluorophore signal from markers for GFP, PV, and WFA, and analyzed signal parameters, that is, optical intensity, volume, and location (Figure S1c). At both 3 and 6 wpi, we observed a large percentage of PV+ interneurons that had abGC mossy fiber labeling within 0.5 μm distance from the cell body surface, as well as a high percentage of PV+ interneurons enwrapped with WFA-labeled PNNs (Figure S1d,e).

We found a positive relationship between PV+ cell PNN intensity and nearby GFP+ bouton number (r = .2632, p = .0255) (Figure 1g; Table S1), where fewer abGC boutons were more often associated with PV+ cells having lower PNN intensities. In order to determine whether axons of new granule cells are more likely to be located near PV+ cells with intense PNNs and with time specificity, we compared abGC mossy fiber bouton number, a more specific measure of putative mossy fiber terminals, using previously determined morphological criteria (Toni et al., 2008), between neighboring pairs of PV+ PNN negative-to-low intensity (neg-low) and PV+ PNN high intensity (high) cells at 3 and 6 wpi timepoints. At 6 wpi, GFP+ bouton number was significantly greater near PV+ cells with high intensity PNNs compared with those with neg-low intensity PNNs in a paired samples t test (t_{15} = 3.784, p = .0018, R^2 = .488) (Figure 1h). This effect was not seen when analyzing 3 wpi GFP+ boutons (t_{26} = 0.4642, p = .6465) (Figure 1h), suggesting that, as previously reported, 3 wpi abGCs exhibit immature connectivity compared to 6 wpi abGCs (Toni et al., 2008). This result suggests a greater likelihood of sustained abGC connectivity with PV+ cells surrounded by more intense PNNs (see depiction, Figure 1i).

To corroborate these findings using an endogenous marker of adult-born neurons, we analyzed 3R-Tau isoform labeling, a microtubule-associated protein found in immature neurons in the DG of the adult mouse brain. 3R-Tau labels the cytoplasm of cell bodies, dendrites, and mossy fibers from abGCs at ~2–7 weeks after their generation (Fuster-Matanzo, Llorens-Martín, Jurado-Arjona, Avila, & Hernández, 2012; Llorens-Martín et al., 2012). 3R-Tau labeling of the DG of adult mice produced numerous stained cells with a morphology and location consistent with adult-generated granule cells (Figure 2a,d). The number of these cells is consistent with those observed using two other commonly used markers of immature neurons in the mouse DG: doublecortin and PSA-NCAM (Bullmann, de Silva, Holzer, Mori, & Arendt, 2007; Llorens-Martín et al., 2012). 3R-Tau labeled mossy fibers were observed emanating from labeled abGCs into the hilar region. Similar to what we observed with GFP-labeled mossy fibers, 3R-Tau labeled axons had characteristic varicosities and were often observed in proximity to PV+ cells in the DG (Figure 2b). We observed a large percentage of PV+ interneurons with 3R-Tau+ abGC mossy fiber labeling within a 0.5 μm distance from the soma (>80%) (Figure S1f), as well as a high percentage of PV+ interneurons enwrapped in PNNs (Figure S1f). Comparison of the two approaches to label abGCs revealed similar staining patterns, with the exception that, as expected, the GFP-retrovirus labeled fewer abGCs than did 3R-Tau. Similar to our results with the retrovirus, the PNN intensity surrounding a PV+ cell shared a positive correlation with the number of 3R-Tau+ boutons located near its cell body, where boutons were less often associated with PV+ interneurons with low PNN intensities (r = .2083, p = .0105) (Figure 2c; Table S2). We also found that 3R-Tau mossy fiber boutons were fewer surrounding PV+ interneurons with neg-low intensity PNNs compared to neighboring interneurons with high intensity PNNs in a paired samples t test (t_{48} = 2.78, p = .0079, R^2 = .1409) (Figure 2e). Again, these results suggest a greater likelihood of sustained abGC connectivity with PV+ cells surrounded by more intense PNNs.

To assess the difference in bouton numbers between neighboring pairs of PV+ interneurons, we calculated a difference score by subtracting the number of boutons associated with the PV+ neg-low PNN cell from that of PV+ high PNN cell and ran a one sample t test to determine whether bouton number significantly differed from chance within the cell pairs. At 3 wpi, the difference in bouton number across pairs did not show a bias toward either the neg-low or high

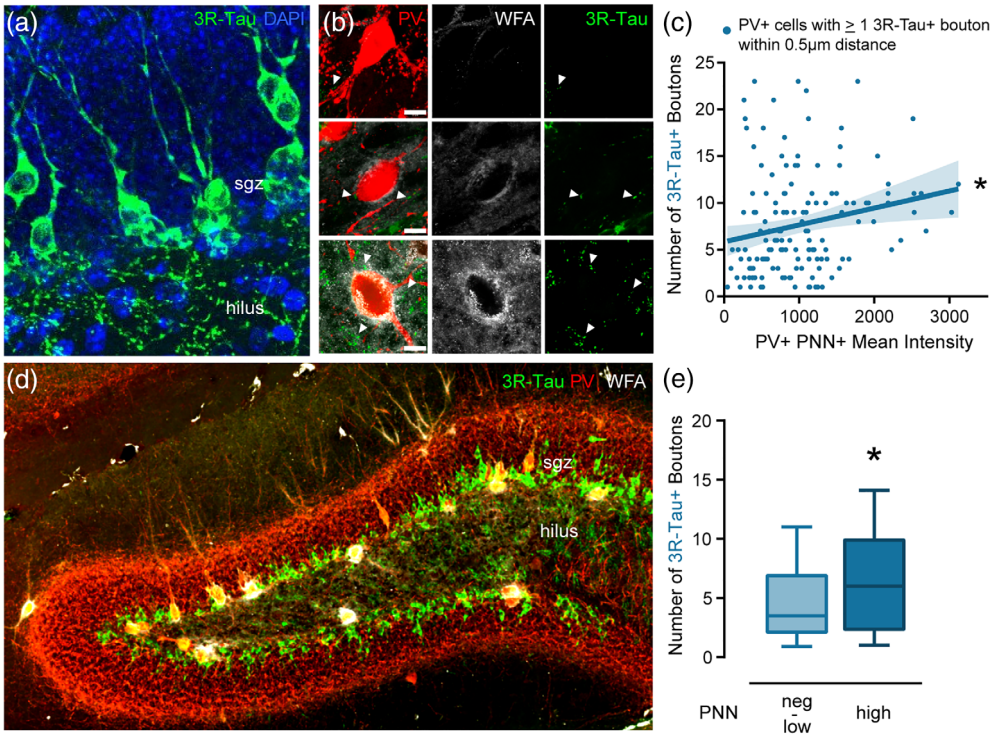

FIGURE 2 3R-Tau labeled abGCs show similar affinity for PV+ PNN+ interneurons as GFP+ retrovirus labeled abGCs. (a). Adult mouse (n = 10) hippocampal sections were immunostained for microtubule-associated protein 3R-Tau (green) and counterstained with DAPI (blue). Representative high magnification image of abGCs and their mossy fibers. (b) Representative high magnification images of PV+ interneurons (red) in the hilus with increasing optical intensities of WFA+ labeled PNNs (white) (top to bottom row), and proximal mossy fibers labeled with 3R-Tau (green). Increased number of 3R-Tau abGC boutons are associated with high-expressing PNNs (bottom row). White arrows indicate mossy fiber bouton examples. Scale bars = 10 μm. (c) Positive correlation between PV+ interneuron PNN optical intensity and number of 3R-Tau+ abGC boutons (r = .2083, p = .0105). (d) Representative image of adult-born neurons labeled with 3R-Tau (green), PV+ interneurons (red), and WFA+ PNNs (white). Scale bar = 50 μm. (e) Paired t test comparison of 3R-Tau+ abGC mossy fiber bouton number within 0.5 μm of the PV+ cell surface, between nearby PV+ interneurons where one cell has weak intensity PNNs (neg-low) and the other has strong intensity PNNs (high). Greater numbers of boutons surrounded strong PNN+ PV+ interneurons compared with neighboring weak PNN+ PV+ interneurons (t_{48} = 2.78, p = .0079). Data are presented as 10–90 percentile box and whisker plots. *p < .05. Related to Figure S1 [Color figure can be viewed at wileyonlinelibrary.com]

cell (t_{25} = 0.4642, p = .6465, mean difference = 0.3077) and was significantly different from 6 wpi (t_{40} = 2.723, p = .0095) (Figure 3a). However, as expected, the 6 wpi and 3R-Tau experiments significantly differed from chance, where both showed a bias toward boutons associated with high compared with neg-low cells (6 wpi: t_{16} = 3.784, p = .0018, mean difference = 3.25; 3R-Tau: t_{47} = 2.777, p = .0079, mean difference = 2.396) (Figure 3a).

It has been previously shown that WFA binds primarily to aggrecan components of PNNs (Giamanco, Morawski, & Matthews, 2010). Aggrecan is a chondroitin sulfate proteoglycan critical for the formation of PNNs, regulated by experience-dependent plasticity, where decreased excitatory input results in decreased PNN formation (McRae, Rocco, Kelly, Brumberg, & Matthews, 2007). Given this information, it is likely that not all PV+ PNN+ interneurons are functionally homogeneous, nor do they share similar PNN profiles. When examining DG PV+ PNN+ interneurons, we found varying levels of WFA intensity, likely representing differing levels of activity-dependent PNN components. We found that cells with higher WFA intensity were also associated with greater abGC mossy fiber intensity (3 wpi: r = .4837, p = .0032; 6 wpi: r = .6535, p < .0001; 3R-Tau: r = .1738, p = .0340) (Figure 3b–d). PV+ protein expression has also been shown to correlate with changes in functional plasticity, that is, coordinated neuronal activity, gamma/theta-band oscillations, and NMDAR activity (Amilhon et al., 2015; Behrens et al., 2007; Korotkova, Fuchs, Ponomarenko, von Engelhardt, & Monyer, 2010; Lodge, Behrens, & Grace, 2009). Therefore, in addition to looking at the relationship between abGCs and PV+ WFA+ PNN intensity, we determined whether a relationship between PV and its surrounding PNN exists by analyzing cell body PV expression using high-resolution confocal imaging. We found that PV+ intensity was also positively associated with WFA+ PNN intensity (3 wpi: r = .8046, p < .0001; 6 wpi: r = .2735, p = .0476; 3R-Tau: r = .1776, p = .0238) (Figure 3e–g), where high-expressing PNNs were likely to surround high-expressing PV+ interneurons, similar to previous published results examining the CA1 region of the hippocampus (Yamada, Ohgomori, & Jinno, 2015).

We discovered that PV+ cells with greater PNN expression were more likely to have nearby immature mossy fiber boutons, retrovirus labeled 6 weeks prior or with endogenous marker 3R-Tau, compared

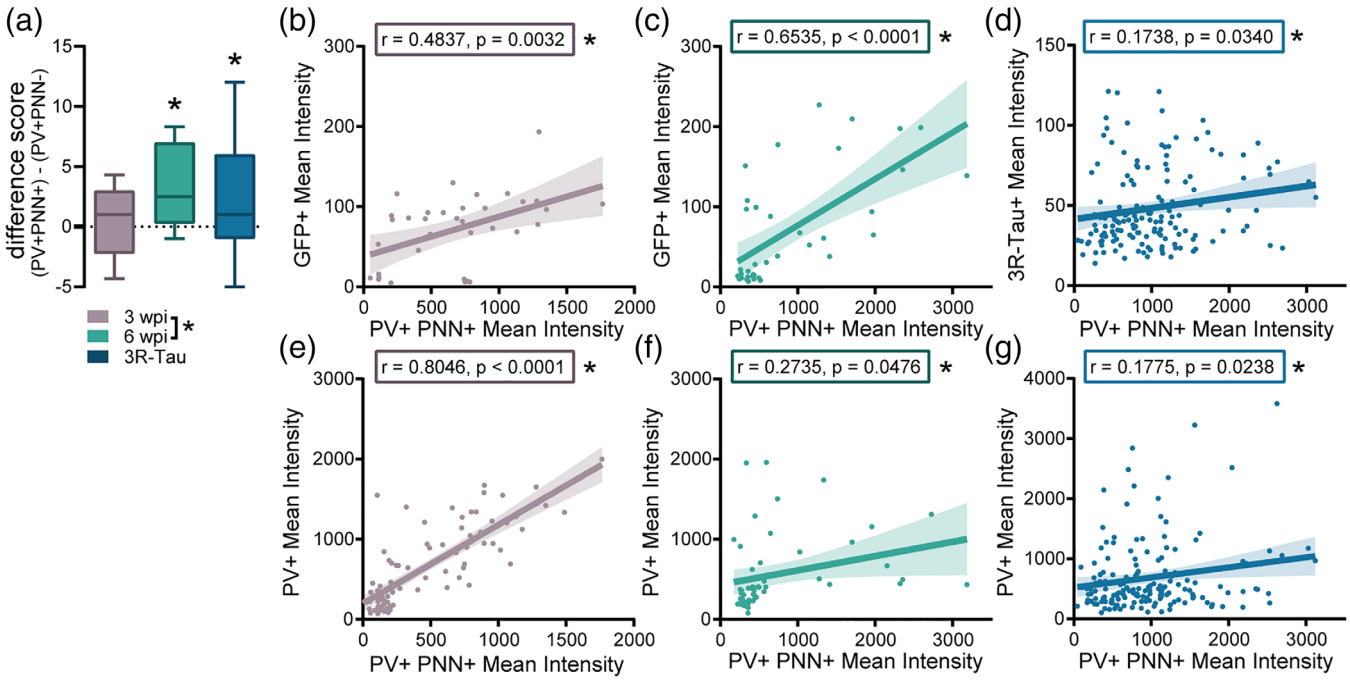

FIGURE 3 Adult-generated mossy fibers prefer PV+ interneurons with high-expressing PNNs, where high-expressing PNNs are also associated with greater PV+ intensity. (a) One sample *t* test analysis of 3, 6 wpi, and 3R-Tau differences in bouton number between PV+ PNN− and PV+ PNN+ interneurons. Paired cells in the 3 wpi experiment did not significantly differ from an at chance difference score (y = 0) (t_{25} = 0.4642, *p* = .6465). Paired cells in the 6 wpi (t_{15} = 3.784, *p* = .0018) and 3R-Tau (t_{47} = 2.78, *p* = .0079) experiments showed positive difference scores, with a significant bouton bias toward the strong intensity PNN+ PV+ interneuron. Unpaired *t* test comparing 3 and 6 wpi difference scores reveal a significant difference between the timepoints (t_{40} = 2.723, *p* = .0095). Data are presented as 10–90 percentile box and whisker plots. (b–d) Positive correlation between mossy fiber mean optical intensity and its surrounding PNN mean optical intensity in the 3 wpi (*r* = .4837, *p* = .0032) (b), 6 wpi (*r* = .6535, *p* < .0001) (c), and 3R-Tau (*r* = .1738, *p* = .034) (d) experiments. (e–g) Positive correlation between PV+ interneuron mean optical intensity and its surrounding PNN mean optical intensity in the 3 wpi (*r* = .4065, *p* < .0001) (e), 6 wpi (*r* = .2735, *p* = .0476) (f), and 3R-Tau (*r* = .1775, *p* = .0238) (g) experiments. **p* < .05 [Color figure can be viewed at wileyonlinelibrary.com]

to neighboring PV+ cells with less intensely stained or no PNN expression. Furthermore, abGC mossy fiber boutons are more likely to be found near PV+ cells with more intensely labeled PNNs, which are also more likely to express PV at higher intensities. Together these findings demonstrate that mossy fibers of abGCs are more likely to be found near PV+ interneurons with PNNs than those without.

3.2 | Transgenic inhibition of adult neurogenesis is associated with fewer PV+ PNN+ interneurons and with less intense PNNs

To test whether the presence of axons from new neurons influences PNN expression around PV+ interneurons, we investigated the densities of PV + PNN+ interneurons in two instances of reduced adult neurogenesis using a transgenic inhibition model and different aged mice. First, we confirmed new neurons were significantly reduced in GFAP-TK mice, a transgenic inducible-knockdown of adult neurogenesis when treated with valganciclovir (vgcv) (Figure 4a), compared with wild-type (WT) and saline-treated controls (ctrl) (β = −78,261.46, *SE* = 9,375.88, *p* < .0001, Cohen's *d* = .6878) (Figure 4b,c; Table S3). Once this difference was determined, we proceeded to compare mice with ablated adult neurogenesis, TK-vgcv, to all three control groups combined. Next, we tested to see if new neuron densities corresponded with PV+ PNN+ cell densities and found that a reduction in new neuron numbers was coincident with a reduction in PV+ PNN+ cell density ($t_{19.86}$ = 2.466, *p* = .0229, Cohen's *d* = .838) (Figure 3d) and a reduction in the percent of total PV+ interneurons surrounded by PNNs (β = −16.20, *SE* = 6.39, *p* = .0188, Cohen's *d* = .360) (Figure S3a). In addition to the observed reduction in PV+ PNN+ cell densities and percent colocalization, we found that transgenic knockout of adult neurogenesis was associated with a reduction in PV+ PNN+ optical intensity (β = 339.21, *SE* = 80.66, *p* = .001, Cohen's d = .237) (Figure 4e). We then examined whether blocking adult neurogenesis affected total PV+ density and PNN+ density separately and found no changes (PV: β = −159.4, *SE* = 242.5, *p* = .517; PNN: β = 9.22, *SE* = 195.4, *p* = .963) (Figure S3a). These results suggest that inhibition of adult neurogenesis is sufficient to reduce PV+ PNNs in both number and intensity.

To follow up the results from the GFAP-TK experiment, we explored whether an age-related reduction in adult neurogenesis (P35 compared with P120 mice) was associated with changes in PNNs surrounding PV+ interneurons. As expected, we found that the density of PSA-NCAM labeled cells was significantly reduced in older mice

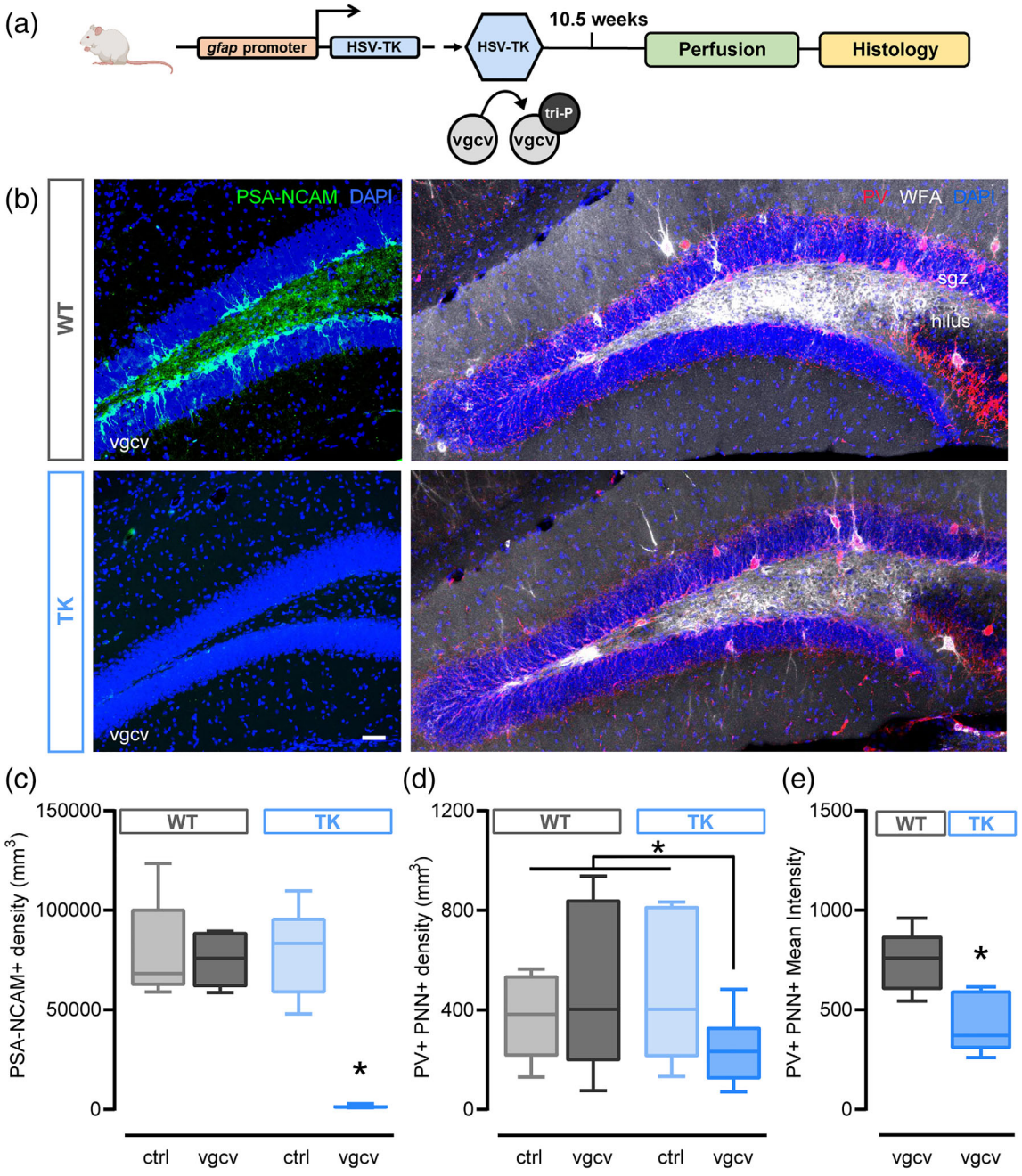

FIGURE 4 Transgenic knockdown of adult neurogenesis is associated with reduced number of PV+ PNN+ neurons in the DG. (a) Representative images of PSA-NCAM labeled adult-born neurons (green) on the left, and PV+ interneurons (magenta), WFA+ PNNs (white), and DAPI (blue) labeled cells on the right. Images displayed are from wild-type (WT, top row) and transgenic (TK, bottom row) mice treated with vgcv. Hilus and sgz = ROIs for cell counts. Scale bar = 50 μm. (b) Adult TK mice were given 10.5 weeks of vgcv (n = 7) before tissue collection and analysis, in addition to littermate controls (n = 7). Aged matched TK mice (n = 7) and littermate controls (n = 5) without vgcv-treatment (ctrl) were also examined in the PSA-NCAM+ and PV+ PNN+ cell density analyses. (c) TK mice treated with vgcv show a robust decrease in PSA-NCAM+ labeled new neurons in comparison with all control groups (β = −78,261.463, SE = 9,375.875, p < .0001). (d) TK mice treated with vgcv compared with all control groups combined, yields a significant decrease in PV+ PNN+ density ($t_{19.86}$ = 2.466, p = .0229). (e) TK mice treated with vgcv have reduced PV+ PNN optical intensity in comparison to WT mice treated with vgcv (β = 339.21, SE = 80.66, p = .001, Cohen's d = .237). Data are presented as 10–90 percentile box and whisker plots. *p < .05. Related to Figure S2 and Figure S3 [Color figure can be viewed at wileyonlinelibrary.com]

(U = 0.0, n_1 = n_2 = 7, p = .0006) (Figure S2b; Table S4), consistent with previous findings (Molofsky et al., 2006). Age-related decline of adult neurogenesis was not, however, coincident with a significant reduction in the number of PV+ PNN+ neurons (β = 283.93, SE = 282.66, p = .335) (Figure S2c). However, we did find that, in older mice, overall PNN+ cell density was decreased (β = 2,136.87,

SE = 461.28, $p < .0005$, Cohen's $d = .478$) (Figure S3b), but the percent of total PV+ interneurons positive for PNNs ($\beta = -0.1967$, *SE* = 9.60, $p = .984$) and PV+ density ($\beta = 310.58$, *SE* = 354.35, $p = .398$) was unchanged (Figure S3b). While these findings suggest that specific near complete reduction of adult neurogenesis is associated with reduced PV+ PNN+ cells, this effect is not evident when the number of new neurons differs for experiential reasons.

3.3 | Running-induced increases in new neuron numbers is associated with reduced numbers of PV+ PNN+ cells

Next, we considered a condition where new neurons were increased in the DG. Consistent with previous results (Schoenfeld et al., 2013; van Praag et al., 1999; van Praag, Shubert, Zhao, & Gage, 2005), we found an increase in adult neurogenesis in mice that had unlimited access to a running wheel compared to sedentary controls ($t_{11.35} = -5.774$, $p = .0001$, Cohen's $d = .404$) (Figure S2e,f; Table S5). However, the running-induced increase in adult neurogenesis was associated with a decrease in PV+ PNN+ density, similar to our transgenic knockdown study ($\beta = -419.47$, *SE* = 183.08, $p = .0417$, Cohen's $d = .193$) (Figure S2g). Surprisingly, running also decreased both the densities of PNN+ cells ($\beta = 1{,}120.9$, *SE* = 446.9, $p = .0144$, Cohen's $d = .478$) and PV+ interneurons ($\beta = -820.0$, *SE* = 311.4, $p = .0103$, Cohen's $d = .6484$) (Figure S3c), separately, suggestive of broader exercise-induced plasticity effects. However, this did not alter the percent of total PV+ interneurons positive for PNNs in runners compared to controls ($\beta = 2.297$, *SE* = 7.276, $p = .758$) (Figure S3c).

The results from these studies suggest that numbers of PV+ interneurons and PNNs may change together. To explore this connection further, we analyzed PV+ density and PNN+ density across all control groups (WT-ctrl and vgcv, TK-ctrl, P35, SED) and found a positive correlation between the two measures ($r = .605$, $p = .00019$). We did not find this to be true when analyzing a correlation between PSA-NCAM + density and PV+ PNN+ density across all control groups ($r = -.022$, $p = .902$). Collectively, these findings suggest that ablation of abGC axons is sufficient to alter PNNs surrounding PV+ interneurons, but do not support the hypothesis that abGC axons are required to stimulate PNN formation around PV+ interneurons. Additionally, it is important to consider that experiential-induced changes to adult neurogenesis, in our studies: aging and exercise, likely induce widespread changes to the hippocampus, many of which are not directly related to abGCs. Given this evidence, it is likely that PNNs reciprocally provide an environment that promotes sustained abGC connectivity.

4 | DISCUSSION

Our findings suggest that axons of abGCs in the DG preferentially target PV+ interneurons with PNNs compared to PV+ interneurons without PNNs. Within the PV+ PNN+ interneuron population, abGC axons are more likely to be located near PV+ interneurons with intense PNNs compared with those with less intense PNNs. It is likely that these results suggest differences in synaptic contact rather than axons in passing, because the relationship was observed with the analysis of GFP+ synaptic boutons, axonal entities found to be colabeled with presynaptic protein synaptophysin. Recent findings have raised the concern that the use of viruses to label and manipulate neurons in the DG may result in the death of abGCs (Johnston et al., 2020). However, our results using an endogenous marker of abGCs, 3R-Tau, closely paralleled those from our retrovirus study, demonstrating that the relationship we observed between abGC axons and PNN+ interneurons is not the result of toxicity or plasticity mechanisms engaged through surgical interventions.

Considerable evidence suggests that PNNs play important roles as general plasticity inhibitors (Faini et al., 2018; Hou et al., 2017; Pizzorusso et al., 2002; Sorg et al., 2016). More specifically, PNNs have been shown to inhibit axonal growth (Wang et al., 2008) and limit receptor movement at hippocampal synapses (Frischknecht et al., 2009). This general view is consistent with recent evidence that PV+ PNN+ interneurons in the DG exhibit less experience-dependent dendritic plasticity than their PV+ PNN− counterparts (Foggetti, Baccini, Arnold, Schiffelholz, & Wulff, 2019). However, recent findings suggest that PNNs also enhance LTP in the hippocampus (Shi et al., 2019), which may increase the impact of innervation by abGCs. Since abGCs have been shown to exhibit enhanced LTP (Snyder, Kee, & Wojtowicz, 2001), it is possible that at synapses which involve postsynaptic targets surrounded by PNNs, that this effect is further augmented. To better understand the role of PNNs in plasticity, many studies have degraded PNNs to determine their effects on brain connectivity. As it stands, the current methodology for transient removal of PNNs is not restricted to PNN components, but rather degrades the entire extracellular matrix, and is known to alter adult neurogenesis (Yamada, Nadanaka, Kitagawa, Takeuchi, & Jinno, 2018), which would produce unintended effects. Given this limitation, our study did not investigate the effects of PNN degradation on abGC synapses on PV+ cells, although future studies using more specific methods should be applied to this question.

In the adult DG, newly generated neurons receive inhibitory input and extend their axons into the hilus, where they primarily target GABAergic inhibitory interneurons (Restivo, Niibori, Mercaldo, Josselyn, & Frankland, 2015; Toni et al., 2008) and form a feedforward inhibitory circuit. Previous studies have demonstrated that individual granule cells possess over 160 varicosities along their mossy fiber collaterals (Claiborne, Amaral, & Cowan, 1986), innervating hilar downstream targets including both GABAergic interneurons and mossy cells, the latter of which are, to our knowledge, not associated with PNNs. Our study focused on comparisons between PV+ expressing cells with and without PNNs, and it remains unknown whether abGC mossy fiber bouton numbers differ between PV+ cells and mossy cells in the DG. While we did not probe this question, it is important to consider that GABAergic interneurons are the major synaptic target of mossy fibers (Ascády, Kamondi, Sík, Freund, & Buzsáki, 1998; Restivo et al., 2015), suggesting that a larger proportion of abGC boutons are likely to be found at or near PV+ cells.

However, future studies are needed to determine the details of this relationship. Since PNN formation varies across the PV+ population, an important consideration is how PNNs influence the activity of the cell. Variation in PNN expression has been shown to be related to input where decreases in PNN expression have been associated with increases in inhibitory input, whereas increases in PNN expression have been associated with increases in excitatory input (Brückner et al., 1993). Recent work has shown that transient removal of PNNs in the anterior cingulate cortex and CA1 region of the hippocampus causes an increase in feedback inhibition onto PV+ interneurons, resulting in impaired theta oscillations. Conversely, increasing PNNs specifically around PV+ interneurons enhanced theta oscillations and improved memory-related behavior (Shi et al., 2019). Additionally, decreased GABAergic signaling was found to be coincident with the downregulation of PV protein expression (Lodge et al., 2009; Volman, Behrens, & Sejnowski, 2011). In parallel, downregulation and upregulation of PV expression have been observed in conjunction with increases in inhibitory input and increases in excitatory input, respectively (Behrens et al., 2007; Filice, Vorckel, Sungur, Wohr, & Schwaller, 2016; Kinney et al., 2006). One interpretation of these results suggests that increased PNN intensity would positively correlate with levels of PV expression, and we found this to be the case in 3 and 6 wpi retrovirus and 3R-Tau labeled tissue.

One possible implication of our finding that abGC axons are more often associated with PV+ PNN+ cells, is that innervation by abGCs drives the formation of PNNs. To investigate this possibility, we examined PNNs in the DG of three different conditions known to alter numbers of abGCs. First, we investigated a GFAP-TK transgenic mouse model of ablated adult neurogenesis and found that mice lacking new neurons in the DG exhibited reduced density of PV+ PNN+ cells and percent colocalization of PV+ cells. These findings are consistent with the hypothesis that abGC innervation may drive increased PNN formation around postsynaptic PV+ targets. Second, we compared mice of two different ages, around the time of puberty and at 4 months of age, where the number of abGCs is known to drop precipitously between these time points. Although we did not detect a significant decrease in the density of PV+ PNN+ cells in the older mice, the mean number of these cells was trending in the expected direction. Unlike the transgenic adult neurogenesis inhibition model, the observed decrease in the number of new neurons in older mice was not a complete reduction and comparatively presented more variation, which may explain the less definitive result in this latter study. Future examination of older mice aged one to two years, with levels of adult neurogenesis more in line with those observed in the transgenic knockout mice, would likely reveal more definitive results. Aging likely involves other major changes in the hippocampus in addition to decreases in the number of abGCs. In this regard, it is worth noting that, although the older mice did not show a convincing reduction in PV+ PNN+ cells, they exhibited a reduction in overall numbers of PNN+ cells, an effect we did not observe in the transgenic mouse model. Furthermore, our aging study shows a slight, but not statistically significant, reduction in PV+ cells, which has been shown to reduce with advanced age (Ueno, Suemitsu, Okamoto, & Ishihara, 2017). Third, we examined whether an experiential condition associated with increased numbers of abGCs, voluntary running, would have an effect on PV+ PNN+ cells. Surprisingly, given our previous results, we found a decrease in numbers of PV+ PNN+ neurons with this comparison, despite substantial increases in the number of abGCs. We also observed a decrease in the overall number of PV+ and PNN+ cells, separately, in the DG of runners, similar to what we observed in the older compared with younger mice. However, we found no difference in the percent of PV+ cells positive for PNNs, an effect we did observe in the transgenic mouse model, suggesting that the reduced numbers of PV+ PNN+ interneurons are likely driven by the observed reduction in PV+ and PNN+ cells in non-overlapping populations. These findings raise the possibility that innervation from abGCs may impact PNN formation around PV+ neurons only when the change in abGCs is specific and near complete.

The interneuron subtypes of PV-negative cells surrounded by PNNs remain elusive, as little to no calretinin+ or somatostatin+ interneurons have been found to be colocalized with PNNs in the hippocampus (Murthy et al., 2019). Thus, the consequences of reduced PV-negative PNN+ cells on hippocampal function in this study remains unknown. It is possible that the manipulations analyzed in this study induce downregulation of PV expression in cells surrounded by PNNs, such that they are no longer detectable as PV+, but future studies are needed to test this. Of course, it is important to consider that both aging and running alter a number of cellular processes, for example, dendritic complexity, synaptic plasticity, and glial cell numbers (Cooper, Moon, & van Praag, 2018; Patterson, 2015), many of which are unlikely to be directly linked to abGCs. Therefore, it remains the case, that the most specific alteration in abGCs—the transgenic model we examined—exhibited reduced PV+ PNN+ cell density and percentage in conjunction with reduced abGCs. Thus, we cannot rule out the hypothesis that abGC innervation onto PV+ interneurons may drive the cell to produce more molecules associated with PNNs. The lack of this effect in the other conditions may be due to the engagement of compensatory or unrelated processes during aging and running.

An alternative, but not mutually exclusive, hypothesis is that PNNs surrounding PV+ interneurons may have chemoattractive properties that guide more abGC axons to grow toward them. Although this hypothesis has not been directly tested, some molecules associated with PNNs, such as semaphorin 3A, a regulator of synaptic inputs (Dick et al., 2013; Vo et al., 2013), or neuronal pentraxin-2, known to regulate and recruit AMPA receptors on PV+ cells (Pelkey et al., 2015), are potential candidates to play this role. Brevican, neurocan, and tenascin PNN components have been shown to be necessary for both excitatory and inhibitory activity (Geissler et al., 2013) and maintenance of synaptic strength in the DG (Jansen et al., 2017), bolstering the claim that PNNs are regulators, not just inhibitors, of plasticity. It could also be the case that PNNs stabilize inputs from abGCs, creating a more preferable environment for maintaining and supporting new synaptic connections. Future studies investigating synaptic connections of mature abGCs (>12 weeks old) with PV+ PNN+ and PV+ PNN− cells would provide added insight into whether preferential connectivity between abGCs and PV+ PNN

+ cells is sustained. It should also be noted that the majority of granule cells in the DG are generated during development (Snyder & Cameron, 2012). The mossy fiber innervation patterns of mature granule cells generated during development would also be interesting to examine regarding PV+ and PNN+ target interneurons. These additional analyses would address whether the preference of mossy fibers to innervate PV+ interneurons with PNNs is a transient feature of abGCs or whether it is a common feature of all granule cells after they reach a certain stage of maturation, regardless of the life stage at which they were born.

This study reveals that axons and boutons of abGCs are more likely to be associated with PV+ cells surrounded by PNNs, and that a positive relationship exists between abGC axons and PNN intensity in the DG. Here, we showed that a large reduction of adult neurogenesis using a transgenic model was sufficient to substantially decrease PV+ PNN+ cell density, intensity, and colocalization, but that a moderate reduction with aging was not, nor was the converse observed with a running-induced increase in new neuron numbers. Together, our results suggest that PNNs surrounding PV+ interneurons within the DG are the preferred targets of abGCs, but the extent, to which this relationship is driven primarily by abGCs, their PNN+ targets, or both, remains to be further explored.

ACKNOWLEDGMENTS

Thanks to the Gould lab members for helpful discussions on the project, and for monitoring mice from the running study.

DATA AVAILABILITY STATEMENT

All code and data that support the findings of this study are available from the corresponding author upon request.

ORCID

Brandy A. Briones https://orcid.org/0000-0003-4692-3399
Thomas J. Pisano https://orcid.org/0000-0002-8432-113X
Esteban A. Engel https://orcid.org/0000-0003-1115-9474
Heather A. Cameron https://orcid.org/0000-0002-3245-5777
Elizabeth Gould https://orcid.org/0000-0002-8358-0236

REFERENCES

Abrous, D. N., & Wojtowicz, J. M. (2015). Interaction between neurogenesis and hippocampal memory system: New vistas. *Cold Spring Harbor Perspectives in Biology*, *7*, a018952. https://doi.org/10.1101/cshperspect.a018952

Akers, K. G., Martinez-Canabal, A., Restivo, L., Yiu, A. P., Cristofaro, A. D., Hsiang, H.-L., … Frankland, P. W. (2014). Hippocampal neurogenesis regulates forgetting during adulthood and infancy. *Science*, *344*, 598–602. https://doi.org/10.1126/science.1248903

Amilhon, B., Huh, C. Y., Manseau, F., Ducharme, G., Nichol, H., Adamantidis, A., & Williams, S. (2015). Parvalbumin interneurons of the hippocampus tune population activity at theta frequency. *Neuron*, *86*, 1277–1289. https://doi.org/10.1016/j.neuron.2015.05.027

Ascády, L., Kamondi, A., Sík, A., Freund, T., & Buzsáki, G. (1998). GABAergic cells are the major postsynaptic targets of mossy fibers in the rat hippocampus. *The Journal of Neuroscience*, *18*, 3386–3403. https://doi.org/10.1523/JNEUROSCI.18-09-03386

Bates, D., Mächler, M., Bolker B., & Walker, S. (2015). Fitting linear mixed-effects models using lme4. *Journal of Statistical Software*, *67*(1), http://dx.doi.org/10.18637/jss.v067.i01.

Behrens, M. M., Ali, S. S., Dao, D. N., Lucero, J., Shekhtman, G., Quick, K. L., & Dugan, L. L. (2007). Ketamine-induced loss of phenotype of fast-spiking interneurons is mediated by NADPH-oxidase. *Science*, *318*, 1645–1647. https://doi.org/10.1126/science.1148045

Brückner, G., Brauer, K., Härtig, W., Wolff, J. R., Rickmann, M. J., Derouiche, A., … Reichenbach, A. (1993). Perineuronal nets provide a polyanionic, glia-associated form of microenvironment around certain neurons in many parts of the rat brain. *Glia*, *8*, 183–200. https://doi.org/10.1002/glia.440080306

Bullmann, T., de Silva, R., Holzer, M., Mori, H., & Arendt, T. (2007). Expression of embryonic tau protein isoforms persist during adult neurogenesis in the hippocampus. *Hippocampus*, *17*, 98–102. https://doi.org/10.1002/hipo.20255

Claiborne, B. J., Amaral, D. G., & Cowan, W. M. (1986). A light and electron microscopic analysis of the mossy fibers of the rat dentate gyrus. *The Journal of Comparative Neurology*, *246*, 435–458. https://doi.org/10.1002/cne.902460403

Cooper, C., Moon, H. Y., & van Praag, H. (2018). On the run for hippocampal plasticity. *Cold Spring Harbor Perspectives in Medicine*, *8*(4), a029736. https://doi.org/10.1101/cshperspect.a029736

Dick, G., Tan, C. L., Alves, J. N., Ehlert, E. M. E., Miller, G. M., Hsieh-Wilson, L. C., … Kwok, J. C. F. (2013). Semaphorin 3A binds to the perineuronal nets via chondroitin sulfate type E motifs in rodent brains. *The Journal of Biological Chemistry*, *288*, 27384–27395. https://doi.org/10.1074/jbc.M111.310029

Dieni, C. V., Gonzalez, J. C., & Overstreet-Wadiche, L. (2019). Multifaceted circuit functions of adult-born neurons. *F1000Res*, *8*, F1000 Faculty Rev-1998. https://doi.org/10.12688/f1000research.20642

Dityatev, A., Brückner, G., Dityateva, G., Grosche, J., Kleene, R., & Schachner, M. (2007). Activity-dependent formation and functions of chondroitin sulfate-rich extracellular matrix of perineuronal nets. *Developmental Neurobiology*, *67*, 570–588. https://doi.org/10.1002/dneu.20361

Faini, G., Aguirre, A., Landi, S., Lamers, D., Pizzorusso, T., Ratto, G. M., … Bacci, A. (2018). Perineuronal nets control visual input via thalamic recruitment of cortical PV interneurons. *eLife*, *7*, e41520. https://doi.org/10.7554/eLife.41520

Favuzzi, E., Marques-Smith, A., Deogracias, R., Winterflood, C. M., Sánchez-Aguilera, A., Mantoan, L., … Rico, B. (2017). Activity-dependent gating of parvalbumin interneuron function by the perineuronal net protein brevican. *Neuron*, *95*, 639–655.e10. https://doi.org/10.1016/j.neuron.2017.06.028

Filice, F., Vorckel, K. J., Sungur, A. O., Wohr, M., & Schwaller, B. (2016). Reduction in parvalbumin expression not loss of parvalbumin-expressing GABA interneuron subpopulation in genetic parvalbumin and shank mouse models of autism. *Molecular Brain*, *9*, 10. https://doi.org/10.1186/s13041-016-0192-8

Foggetti, A., Baccini, G., Arnold, P., Schiffelholz, T., & Wulff, P. (2019). Spiny and non-spiny parvalbumin-positive hippocampal interneurons show different plastic properties. *Cell Reports*, *27*, 3725–3732.e5. https://doi.org/10.1016/j.celrep.2019.05.098

Freund, T. F., & Buzsáki, G. (1996). Interneurons of the hippocampus. *Hippocampus*, *6*, 347–470. https://doi.org/10.1002/(SICI)1098-1063(1996)6:4<347::AID-HIPO1>3.0.CO;2-I

Frischknecht, R., Heine, M., Perrais, D., Seidenbecher, C. I., Choquet, D., & Gundelfinger, E. D. (2009). Brain extracellular matrix affects AMPA receptor lateral mobility and short-term synaptic plasticity. *Nature Neuroscience*, *12*, 897–904. https://doi.org/10.1038/nn.2338

Fuster-Matanzo, A., Llorens-Martín, M., Jurado-Arjona, J., Avila, J., & Hernández, F. (2012). Tau protein and adult hippocampal neurogenesis. *Frontiers in Neuroscience*, *6*, 104. https://doi.org/10.3389/fnins.2012.00104

Geissler, M., Gottschling, C., Aguado, A., Rauch, U., Wetzel, C. H., Hatt, H., & Faissner, A. (2013). Primary hippocampal neurons, which lack four crucial extracellular matrix molecules, display abnormalities of synaptic structure and function and severe deficits in perineuronal net formation. *The Journal of Neuroscience*, *33*, 7742–7755. https://doi.org/10.1523/JNEUROSCI.3275-12.2013

Giamanco, K. A., Morawski, M., & Matthews, R. T. (2010). Perineuronal net formation and structure in aggrecan knockout mice. *Neuroscience*, *170*, 1314–1327. https://doi.org/10.1016/j.neuroscience.2010.08.032

Harris, C. R., Jarrod Millman, K., van der Walt, S. J., Gommers, R., Virtanen, P., Cournapeau, D., & Oliphant, T. E. (2020) Array programming with NumPy, *Nature*, *585*, 357–362. https://doi.org/10.1038/s41586-020-2649-2

Hou, X., Yoshioka, N., Tsukano, H., Sakai, A., Miyata, S., Watanabe, Y., … Sugiyama, S. (2017). Chondroitin sulfate is required for onset and offset of critical period plasticity in visual cortex. *Scientific Reports*, *7*, 1–17. https://doi.org/10.1038/s41598-017-04007-x

Howerton, D. L., Garner, J. P., & Mench, J. A. (2008). Effects of a running wheel—Igloo enrichment on aggression, hierarchy linearity, and stereotypy in group-housed male CD1 (ICR) mice. *Applied Animal Behaviour Science*, *115*, 90–103. https://doi.org/10.1016/j.applanim.2008.05.004

Ikrar, T., Guo, N., He, K., Besnard, A., Levinson, S., Hill, A., … Sahay, A. (2013). Adult neurogenesis modifies excitability of the dentate gyrus. *Frontiers in Neural Circuits*, *7*, 204. https://doi.org/10.3389/fncir.2013.00204

Jansen, S., Gottschling, C., Faissner, A., & Manahan-Vaughan, D. (2017). Intrinsic cellular and molecular properties of in vivo hippocampal synaptic plasticity are altered in the absence of key synaptic matrix molecules. *Hippocampus*, *27*, 920–933. https://doi.org/10.1002/hipo.22742

Johnston, S. T., Parylak, S. L., Kim, S., Mac, N., Lim, C. K., Gallina, I. S., … Shtrahman, M. (2020). AAV ablates neurogenesis in the adult murine hippocampus. *bioRxiv*, *19*, 2020. https://doi.org/10.1101/2020.01.18.911362

Kaliste, E. K., Mering, S. M., & Huuskonen, H. K. (2006). Environmental modification and agonistic behavior in NIH/S male mice: Nesting material enhances fighting but shelters prevent it. *Comparative Medicine*, *56*, 202–208.

Kinney, J. W., Davis, C. N., Tabarean, I., Conti, B., Bartfai, T., & Behrens, M. M. (2006). A specific role for NR2A-containing NMDA receptors in the maintenance of parvalbumin and GAD67 immunoreactivity in cultured interneurons. *The Journal of Neuroscience*, *5*, 1604–1615. https://doi.org/10.1523/JNEUROSCI.4722-05.2006

Korotkova, T., Fuchs, E. C., Ponomarenko, A., von Engelhardt, J., & Monyer, H. (2010). NMDA receptor ablation on parvalbumin-positive interneurons impairs hippocampal synchrony, spatial representations, and working memory. *Neuron*, *68*, 557–569. https://doi.org/10.1016/j.neuron.2010.09.017

Laplagne, D. A., Espósito, M. S., Piatti, V. C., Morgenstern, N. A., Zhao, C., van Praag, H., … Schinder, A. F. (2006). Functional convergence of neurons generated in the developing and adult hippocampus. *PLoS Biology*, *4*, e409. https://doi.org/10.1371/journal.pbio.0040409

Lensjø, K. K., Christensen, A. C., Tennøe, S., Fyhn, M., & Hafting, T. (2017). Differential expression and cell-type specificity of perineuronal nets in hippocampus, medial entorhinal cortex, and visual cortex examined in the rat and mouse. *eNeuro*, *4*, 379–316. https://doi.org/10.1523/ENEURO.0379-16.2017

Llorens-Martín, M., Jurado-Arjona, J., Avila, J., & Hernández, F. (2015). Novel connection between newborn granule neurons and the hippocampal CA2 field. *Experimental Neurology*, *263*, 285–292. https://doi.org/10.1016/j.expneurol.2014.10.021

Llorens-Martín, M., Teixeira, C. M., Fuster-Matanzo, A., Jurado-Arjona, J., Borrell, V., Soriano, E., … Hernández, F. (2012). Tau isoform with three microtubule binding domains is a marker of new axons generated from the subgranular zone in the hippocampal dentate gyrus: Implications for alzheimer's disease. *Journal of Alzheimer's Disease*, *29*, 921–930. https://doi.org/10.3233/JAD-2012-112057

Lodge, D. J., Behrens, M. M., & Grace, A. A. (2009). A loss of parvalbumin-containing interneurons is associated with diminished oscillatory activity in an animal model of schizophrenia. *The Journal of Neuroscience*, *29*, 2344–2354. https://doi.org/10.1523/JNEUROSCI.5419-08.2009

Lowekamp, B. C., Chen, D. T., Ibáñez, L., & Blezek, D. (2013). The design of simpleitk. *Frontiers in Neuroinformatics*, *7*, 45. https://doi.org/10.3389/fninf.2013.00045

Luna, V. M., Anacker, C., Burghardt, N. S., Khandaker, H., Andreu, V., Millette, A., … Hen, R. (2019). Adult-born hippocampal neurons bidirectionally modulate entorhinal inputs into the dentate gyrus. *Science*, *364*, 578–583. https://doi.org/10.1126/science.aat8789

Marín-Burgin, A., Mongiat, L. A., Pardi, M. B., & Schinder, A. F. (2012). Unique processing during a period of high excitation/inhibition balance in adult-born neurons. *Science*, *335*, 1238–1242. https://doi.org/10.1126/science.1214956

McKinney, W. (2010). Data structures for statistical computing in python. *Proceedings of the 9th Python in Science Conference*, *445*, 51–56.

McRae, P. A., Rocco, M. M., Kelly, G., Brumberg, J. C., & Matthews, R. T. (2007). Sensory deprivation alters aggrecan and perineuronal net expression in the mouse barrel cortex. *The Journal of Neuroscience*, *27*, 5405–5413. https://doi.org/10.1523/JNEUROSCI.5425-06.2007

Molofsky, A. V., Slutsky, S. G., Joseph, N. M., He, S., Pardal, R., Krishnamurthy, J., … Morrison, S. J. (2006). Increasing p16INK4a expression decreases forebrain progenitors and neurogenesis during ageing. *Nature*, *443*, 448–452. https://doi.org/10.1038/nature05091

Murthy, S., Kane, G. A., Katchur, N. J., Mejia, P. S. L., Obiofuma, G., Buschman, T. J., … Gould, E. (2019). Perineuronal nets, inhibitory interneurons, and anxiety-related ventral hippocampal neuronal oscillations are altered by early life adversity. *Biological Psychiatry*, *85*, 1011–1020. https://doi.org/10.1016/j.biopsych.2019.02.021

Opendak, M., Offit, L., Monari, P., Schoenfeld, T. J., Sonti, A. N., Cameron, H. A., & Gould, E. (2016). Lasting adaptations in social behavior produced by social disruption and inhibition of adult neurogenesis. *The Journal of Neuroscience*, *36*, 7027–7038. https://doi.org/10.1523/JNEUROSCI.4435-15.2016

Patterson, S. L. (2015). Immune dysregulation and cognitive vulnerability in the aging brain: Interactions of microglia, IL-1β, BDNF and synaptic plasticity. *Neuropharmacology*, *96*, 11–18. https://doi.org/10.1016/j.neuropharm.2014.12.020

Paxinos, G., & Franklin, K. B. J. (2008). *The mouse brain in stereotaxic coordinates: Hard cover* (3rd ed.) Cambridge, MA: Academic Press.

Pelkey, K. A., Barksdale, E., Craig, M. T., Yuan, X., Sukumaran, M., Vargish, G. A., … McBain, C. J. (2015). Pentraxins coordinate excitatory synapse maturation and circuit integration of parvalbumin interneurons. *Neuron*, *85*, 1257–1272. https://doi.org/10.1016/j.neuron.2015.02.020

Pizzorusso, T., Medini, P., Berardi, N., Chierzi, S., Fawcett, J. W., & Maffei, L. (2002). Reactivation of ocular dominance plasticity in the adult visual cortex. *Science*, *298*, 1248–1251. https://doi.org/10.1126/science.1072699

Restivo, L., Niibori, Y., Mercaldo, V., Josselyn, S. A., & Frankland, P. W. (2015). Development of adult-generated cell connectivity with excitatory and inhibitory cell populations in the hippocampus. *The Journal of Neuroscience*, *35*, 10600–10612. https://doi.org/10.1523/JNEUROSCI.3238-14.2015

RStudio Team. (2020). *RStudio: Integrated Development Environment for R*. Boston, MA: RStudio, PBC, http://www.rstudio.com/ .

Sah, N., Peterson, B. D., Lubejko, S. T., Vivar, C., & van Praag, H. (2017). Running reorganizes the circuitry of one-week-old adult-born hippocampal neurons. *Scientific Reports*, *7*, 10903. https://doi.org/10.1038/s41598-017-11268-z

Sahay, A., Scobie, K. N., Hill, A. S., O'Carroll, C. M., Kheirbek, M. A., Burghardt, N. S., … Hen, R. (2011). Increasing adult hippocampal neurogenesis is sufficient to improve pattern separation. *Nature*, *472*, 466–470. https://doi.org/10.1038/nature09817

Schindelin, J., Arganda-Carreras, I., Frise, E., Kaynig, V., Longair, M., Pietzsch, T., … Cardona, A. (2012). Fiji: An open-source platform for biological-image analysis. *Nature Methods*, *9*, 676–682. https://doi.org/10.1038/nmeth.2019

Schoenfeld, T. J., Rada, P., Pieruzzini, P. R., Hsueh, B., & Gould, E. (2013). Physical exercise prevents stress-induced activation of granule neurons and enhances local inhibitory mechanisms in the dentate gyrus. *The Journal of Neuroscience*, *33*, 7770–7777. https://doi.org/10.1523/JNEUROSCI.5352-12.2013

Schüppel, K., Brauer, K., Härtig, W., Grosche, J., Earley, B., Leonard, B. E., & Brückner, G. (2002). Perineuronal nets of extracellular matrix around hippocampal interneurons resist destruction by activated microglia in trimethyltin-treated rats. *Brain Research*, *958*, 448–453. https://doi.org/10.1016/s0006-8993(02)03569-2

Shi, W., Wei, X., Wang, X., Du, S., Liu, W., Song, J., & Wang, Y. (2019). Perineuronal nets protect long-term memory by limiting activity-dependent inhibition from parvalbumin interneurons. *Proceedings of the National Academy of Sciences*, *116*, 27063–27073. https://doi.org/10.1073/pnas.1902680116

Snyder, J. S., & Cameron, H. A. (2012). Could adult hippocampal neurogenesis be relevant for human behavior? *Behavioural Brain Research*, *227*(2), 384–390. https://pubmed.ncbi.nlm.nih.gov/21736900/.

Snyder, J. S., Kee, N., & Wojtowicz, J. M. (2001). Effects of adult neurogenesis on synaptic plasticity in the rat dentate gyrus. *Journal of Neurophysiology*, *85*, 2423–2431. https://doi.org/10.1152/jn.2001.85.6.2423

Snyder, J. S., Soumier, A., Brewer, M., Pickel, J., & Cameron, H. A. (2011). Adult hippocampal neurogenesis buffers stress responses and depressive behaviour. *Nature*, *476*, 458–461. https://doi.org/10.1038/nature10287

Song, J., Sun, J., Moss, J., Wen, Z., Sun, G. J., Hsu, D., … Song, H. (2013). Parvalbumin interneurons mediate neuronal circuitry–neurogenesis coupling in the adult hippocampus. *Nature Neuroscience*, *16*, 1728–1730. https://doi.org/10.1038/nn.3572

Sorg, B. A., Berretta, S., Blacktop, J. M., Fawcett, J. W., Kitagawa, H., Kwok, J. C. F., & Miquel, M. (2016). Casting a wide net: Role of perineuronal nets in neural plasticity. *The Journal of Neuroscience*, *36*, 11459–11468. https://doi.org/10.1523/JNEUROSCI.2351-16.2016

Stewart, S. A., Dykxhoorn, D. M., Palliser, D., Mizuno, H., Yu, E. Y., An, D. S., … Novina, C. D. (2003). Lentivirus-delivered stable gene silencing by RNAi in primary cells. *RNA*, *9*, 493–501. https://doi.org/10.1261/rna.2192803

Sullivan, H. A., & Wickersham, I. R. (2015). Concentration and purification of rabies viral and lentiviral vectors. *Cold Spring Harbor Protocols*, *2015*(4), 386–391. https://doi.org/10.1101/pdb.prot075887

Toni, N., Laplagne, D. A., Zhao, C., Lombardi, G., Ribak, C. E., Gage, F. H., & Schinder, A. F. (2008). Neurons born in the adult dentate gyrus form functional synapses with target cells. *Nature Neuroscience*, *11*, 901–907. https://doi.org/10.1038/nn.2156

Ueno, H., Suemitsu, S., Okamoto, M., & Ishihara, T. (2017). Parvalbumin neurons and perineuronal nets in the mouse prefrontal cortex. *Neuroscience*, *343*, 115–127. https://doi.org/10.1016/j.neuroscience.2016.11.035

van der Walt, S., Schönberger, J. L., Nunez-Iglesias, J., Boulogne, F., Warner, J. D., Yager, N., … Yu, T. (2014). Scikit-image: Image processing in python. *PeerJ*, *2*, e453. https://doi.org/10.7717/peerj.453

van Praag, H., Kempermann, G., & Gage, F. H. (1999). Running increases cell proliferation and neurogenesis in the adult mouse dentate gyrus. *Nature Neuroscience*, *2*, 266–270. https://doi.org/10.1038/6368

van Praag, H., Shubert, T., Zhao, C., & Gage, F. H. (2005). Exercise enhances learning and hippocampal neurogenesis in aged mice. *The Journal of Neuroscience*, *25*, 8680–8685. https://doi.org/10.1523/JNEUROSCI.1731-05.2005

Virtanen, P., Gommers, R., Oliphant, T. E., Haberland, M., Reddy, T., Cournapeau, D., … SciPy 1.0 Contributors, (2020). SciPy 1.0: fundamental algorithms for scientific computing in python. *Nature Methods*, *17*(3), 261–272.

Vivar, C., Peterson, B. D., & van Praag, H. (2016). Running rewires the neuronal network of adult-born dentate granule cells. *NeuroImage*, *131*, 29–41. https://doi.org/10.1016/j.neuroimage.2015.11.031

Vo, T., Carulli, D., Ehlert, E. M. E., Kwok, J. C. F., Dick, G., Mecollari, V., … Verhaagen, J. (2013). The chemorepulsive axon guidance protein semaphorin3A is a constituent of perineuronal nets in the adult rodent brain. *Molecular and Cellular Neurosciences*, *56*, 186–200. https://doi.org/10.1016/j.mcn.2013.04.009

Volman, V., Behrens, M. M., & Sejnowski, T. J. (2011). Downregulation of parvalbumin at cortical gaba synapses reduces network gamma oscillatory activity. *The Journal of Neuroscience*, *31*, 18137–18148. https://doi.org/10.1523/JNEUROSCI.3041-11.2011

Wang, H., Katagiri, Y., McCann, T. E., Unsworth, E., Goldsmith, P., Yu, Z.-X., … Geller, H. M. (2008). Chondroitin-4-sulfation negatively regulates axonal guidance and growth. *Journal of Cell Science*, *121*, 3083–3091. https://doi.org/10.1242/jcs.032649

Yamada, J., Nadanaka, S., Kitagawa, H., Takeuchi, K., & Jinno, S. (2018). Increased synthesis of chondroitin sulfate proteoglycan promotes adult hippocampal neurogenesis in response to enriched environment. *The Journal of Neuroscience*, *38*, 8496–8513. https://doi.org/10.1523/JNEUROSCI.0632-18.2018

Yamada, J., Ohgomori, T., & Jinno, S. (2015). Perineuronal nets affect parvalbumin expression in GABAergic neurons of the mouse hippocampus. *The European Journal of Neuroscience*, *41*, 368–378. https://doi.org/10.1111/ejn.12792

Zhao, C., Teng, E. M., Summers, R. G., Ming, G., & Gage, F. H. (2006). Distinct morphological stages of dentate granule neuron maturation in the adult mouse hippocampus. *The Journal of Neuroscience*, *26*, 3–11. https://doi.org/10.1523/JNEUROSCI.3648-05.2006

SUPPORTING INFORMATION

Additional supporting information may be found online in the Supporting Information section at the end of this article.

How to cite this article: Briones BA, Pisano TJ, Pitcher MN, et al. Adult-born granule cell mossy fibers preferentially target parvalbumin-positive interneurons surrounded by perineuronal nets. *Hippocampus*. 2021;1–14. https://doi.org/10.1002/hipo.23296